Effect of stray magnetic fields on particles in the Wendelstein 7-X neutral beam box

L. van Ham[1], S.A. Lazerson[2], B.C. Hamstra[3], P. McNeely[1], N. Rust[1], D. Hartmann[1], S. Bozhenkov[1], and the Wendelstein 7-X Team[4]

[1] *Max Planck Institute for Plasma Physics, Greifswald, Germany*

[2] *Gauss Fusion GmbH, Garching, Germany*

[3] *Eindhoven University of Technology, Eindhoven, The Netherlands*

[4] *See author list of O. Grulke et al 2024 Nucl. Fusion **64** 112002*

Introduction. Neutral Beam Injection (NBI) is a critical tool at the Wendelstein 7-X (W7-X) stellarator for plasma heating, diagnostics, and plasma studies. The W7-X NBI systems consist of two NBI boxes, NI20 and NI21, each containing two 5 MW RF ion sources (sources 3 and 4 in NI20, sources 7 and 8 in NI21). NBI beams and and heat loads are observed to shift when the main W7-X magnetic field is active, suggesting that stray magnetic fields penetrate the NBI boxes through their magnetic shielding. In this contribution, we investigate the magnetic field inside the NI21 box using the magnetic materials model MUMAT. The Monte Carlo particle following code BEAMS3D [1] is used to simulate particle trajectories through the magnetic field and determine its effect on heat load patterns.

Development of MUMAT. MUMAT is a Finite-Element Method (FEM) code based on the mathematical formalism of MagTense [2]. Within this formalism, a volume of magnetically permeable material is discretized into a 3-D mesh of tetrahedral elements, where each element i has uniform magnetization $\boldsymbol{M}_i$, producing a magnetic field $\boldsymbol{H_i}(\boldsymbol{r}) = \mathrm{N}_i(\boldsymbol{r}) \cdot \boldsymbol{M}_i$, where $\mathrm{N}_i(r)$ is the 3-by-3 demagnetization tensor of the element at position $\boldsymbol{r}$. The magnetization of element i is described by a state function $\boldsymbol{M}_i = \boldsymbol{M}\big(\boldsymbol{H}(\boldsymbol{r}_i)\big)$. A double Picard scheme is used to determine the magnetization of all elements: one loop acts to determine the magnetization of an element in response to a background field, other magnetized elements, and its self-field; a second loop iterates over all elements until all magnetizations converge, after which the magnetic field can be determined everywhere in space. The code has a distance-based cut-off beyond which elements are treated as dipoles, and is also MPI-parallelized. For verification purposes, a magnetically permeable shell ($r_1 = 0.5$ m, $r_2 = 1$ m, $\mu_r = 500$) is subjected to a background magnetic field ($\boldsymbol{B} = B_0\hat{z}, B_0 = 1$ T). This problem has a known analytical magnetic field. The problem is recreated within MUMAT and results are shown in Figure 1. The MUMAT magnetic field is in agreement with the analytical field, differing by <1% for $r > r_2$ and by <1.5% for

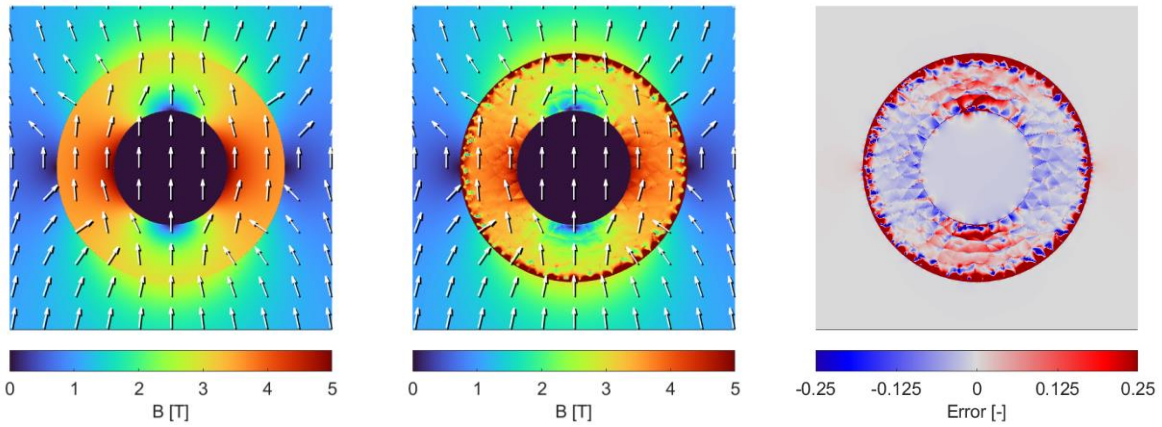

Fig 1. Results of MUMAT verification: (left) analytical magnetic field, (middle) magnetic field as predicted by MUMAT, (right) error in MUMAT magnetic field strength compared to analytical solution.

$r < r_1$. Disagreement within the material is primarily attributed to the finite mesh resolution. Overall, results verify the numerical implementation of MUMAT.

Magnetic field inside NI21. The magnetic materials of the W7-X NBI systems are simplified, discretized, and assigned magnetic properties determined from third-party testing of ARMCO steel. Three scenarios are considered: (1) Bending magnets of the NBI systems are powered with standard operational currents (671.9 A) and no background magnetic field is active; (2) Bending magnets are active and the W7-X forward high-iota configuration is active; (3) Bending magnets are active and the W7-X reversed high-iota configuration is active. These W7-X configurations produce strong fields near the NBI systems. The fields inside NI21 for cases (1) and (2) are shown in Figure 2; the field for case (3) is very similar to case (2), except its direction is primarily radially inwards rather than outwards. Results indicate that significant fields are present throughout NI21 only when the W7-X magnetic field is active. Stray fields enter NI21 through the gap in magnetic shielding and extend over almost the entire box. The magnetic field strength varies between 0.2 – 1.1 mT over the length of the source 7 and source

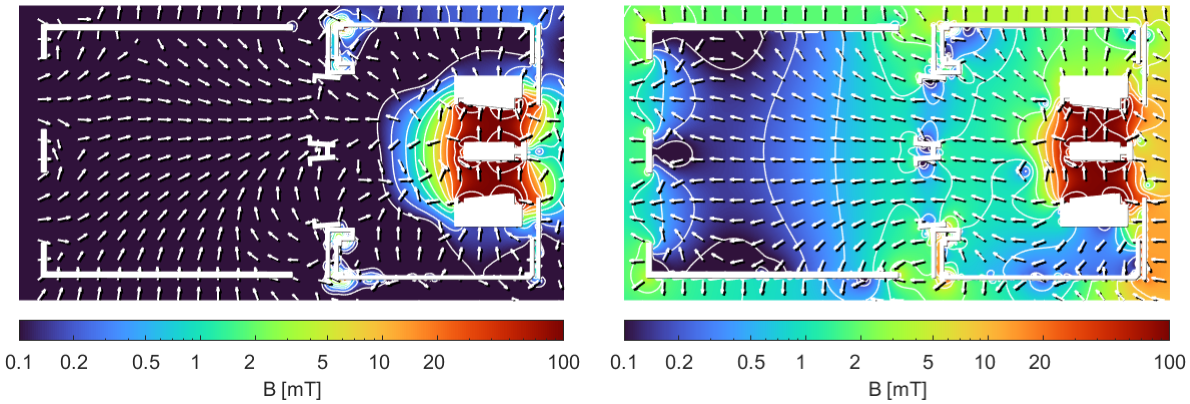

Fig 2. Magnetic field strength inside NI21 box at $z = 0.8$ m (representative of beam height) for cases (1) (left) and (2) (right). White areas indicate magnetic material. Arrows show the direction of magnetic field only.

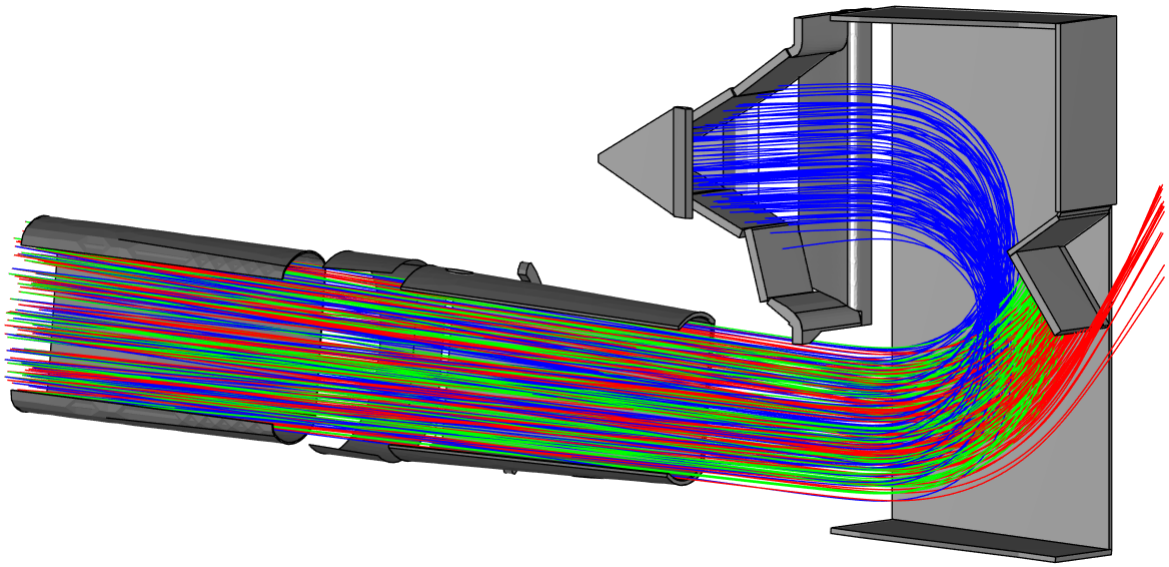

Fig 3. Sample of source 7 charged particle trajectories for case (1). $H^+$is shown in blue, H_2^+ in green, H_3^+ in red. A cut-through of the neutralizer, bending magnet liner, molecular dump, and ion dump are shown.

8 neutralizers, indicating that the field may affect the overall trajectory of neutral particles.

Particle following with BEAMS3D. Source 7 and 8 hydrogen particles (H^+, H_2^+, H_3^+) are followed through the magnetic fields of the three cases with BEAMS3D from the ion sources until they strike a NBI component or leave the domain. Each beam is assigned 1 MW of power for simplicity. Charge exchange is not modeled. Figure 3 shows the trajectories of source 7 particles for case (1). As by NBI design, H^+ particles strike the ion dump, H_2^+ particles strikes the molecular dump, and H_3^+ particles are scraped by the molecular dump. These trajectories validate the magnetic field calculations of MUMAT for this geometry.

The effect of the W7-X magnetic field on the BEAMS3D ion dump heat loads is shown in Figure 4. Without the background field, the heat loads are centered on the ion dump. With the

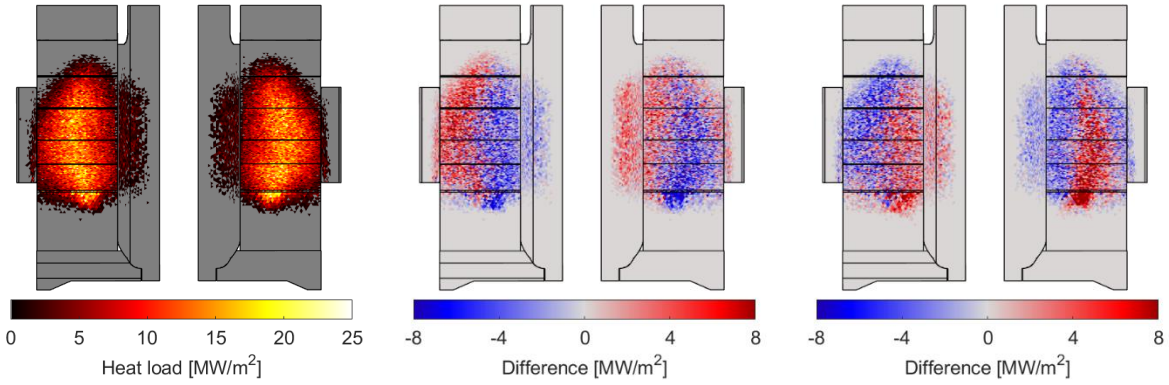

Fig 4. Effect of background W7-X magnetic field on BEAMS3D heat loads on the source 7 and source 8 ion dumps. (left) heat loads for case (1), (middle) difference between heat load of case (2) and case (1), (right) difference between heat load of case (3) and case (1).

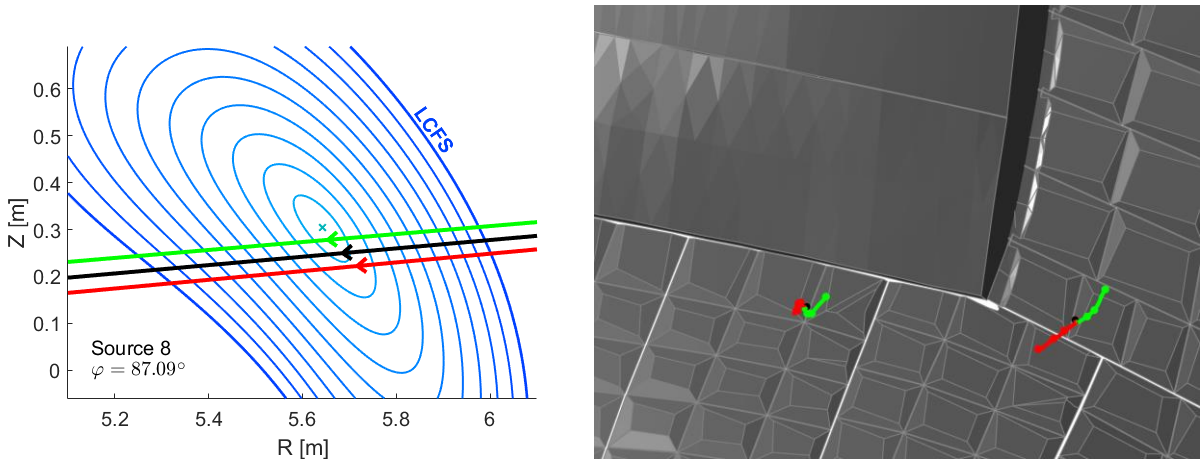

Fig 5. Estimated effect of W7-X magnetic field on NI21 neutral beams. (left) shift of source 8 beam axis, (right) NI21 strike positions in beam dump region. Black lines correspond to case (1), green lines to case (2), and red lines to case (3). Markers indicate neutralizations at the 1/3rd, 2/3^{rds}, and full neutralizer distance.

W7-X forward field, heat loads are shifted up and counterclockwise; with the reversed field, the shift is in the opposite direction. Source 8 experiences a (de)focusing on the beam depending on the polarity of the magnetic field. The vertical shifts are also seen in experiment.

To investigate the effect of the magnetic field on neutral particles, a ray is cast from the average particle position parallel to the average velocity of particles at different distances along the neutralizer. As particles travel further, their injection angle changes and their beams shift inside the vessel. This is visible in Figure 5, where a shift is visible in both the beam passing through the plasma cross-section (left) and in the NI21 beam dump region (right). The shift of source 8 beams is also seen in spectroscopy [3] and in beam dump thermocouple signals. These shifts are somewhat counteracted in experiment by beam steering.

Overall, these calculations produce results which qualitatively agree with observations. A quantitive comparison with experimental data is now foreseen to further validate MUMAT for W7-X. Following this, the codes can be used to help develop new NBI geometries or scenarios.

Acknowledgement.

This work has been carried out within the framework of the EUROfusion Consortium, funded by the European Union via the Euratom Research and Training Programme (Grant Agreement No 101052200 — EUROfusion). Views and opinions expressed are however those of the author(s) only and do not necessarily reflect those of the European Union or the European Commission. Neither the European Union nor the European Commission can be held responsible for them.

References

[1] M. McMillan, S.A. Lazerson 2014 *Plasma Phys. Control. Fusion* **56** 095019

[2] R Bjørk *et al.* 2021 *J. Magn. Magn. Mater*. **535** 168057

[3] S. Bannmann *et al.* 2023 *J. Instrum.* **18** 10029